Real-Time Observation of Iodide Ion Migration in Methylammonium Lead Halide Perovskites

Cheng Li, Antonio Guerrero, Yu Zhong, Anna Gräser, Carlos Andres Melo Luna, Jürgen Köhler, Juan Bisquert, Richard Hildner, and Sven Huettner*

Organic–inorganic metal halide perovskites (e.g., $CH_3NH_3PbI_{3-x}Cl_x$) emerge as a promising optoelectronic material. However, the Shockley–Queisser limit for the power conversion efficiency (PCE) of perovskite-based photovoltaic devices is still not reached. Nonradiative recombination pathways may play a significant role and appear as photoluminescence (PL) inactive (or dark) areas on perovskite films. Although these observations are related to the presence of ions/defects, the underlying fundamental physics and detailed microscopic processes, concerning trap/defect status, ion migration, etc., still remain poorly understood. Here correlated wide-field PL microscopy and impedance spectroscopy are utilized on perovskite films to in situ investigate both the spatial and the temporal evolution of these PL inactive areas under external electric fields. The formation of PL inactive domains is attributed to the migration and accumulation of iodide ions under external fields. Hence, we are able to characterize the kinetic processes and determine the drift velocities of these ions. In addition, it is shown that I_2 vapor directly affects the PL quenching of a perovskite film, which provides evidence that the migration/segregation of iodide ions plays an important role in the PL quenching and consequently limits the PCE of organometal halide-based perovskite photovoltaic devices.

Inorganic–organic metal halide perovskite solar cells (e.g., $CH_3NH_3PbI_{3-x}Cl_x$ and $CH_3NH_3PbI_3$) have achieved remarkable power conversion efficiencies (PCEs) in the last few years, soaring from 3.8%[1] to more than 20%.[2] Yet, quite a lot of fundamental physics in this material is still under debate.[3,4] Among them, more and more concern is concentrated on the

further improvement of PCE approaching the Shockley–Queisser limit.[5]

It is well known that the PCE of solar cells is correlated with their photoluminescence (PL) properties, which is an indication of the charge carrier recombination pathway.[6] Briefly, the charge carrier recombination is considered as a combined process of (1) trap/defect-assisted (first order), (2) electron–hole bimolecular (second order), and (3) Auger recombination (third order).[7,8] To achieve the ideal maximum PCE, or the Shockley–Queisser limit,[9] the device has to perform as a "good radiator,"[10] that is, to maximize the radiative bimolecular recombination based on the detailed balance model. Indeed, perovskites have demonstrated outstanding performance in light emitting diodes[11,12] and lasers.[4,13] Nevertheless, the appearance of dark areas, or PL inactive domains in perovskite films, has been reported.[14–19] These dark areas in PL images indicate the existence of nonradiative recombination pathways, which are detrimental to the energy conversion and can be passivated by chemical treatment.[8,14,20] Recently, more and more evidences demonstrate that this nonradiative recombination is associated with the migration/segregation of ions in the film.[18,21] Therefore, the study of ionic dynamic becomes an emergent issue.

Dr. C. Li, Y. Zhong, A. Gräser, Prof. S. Huettner
Organic and Hybrid Electronics
Macromolecular Chemistry I
University of Bayreuth
Universitätstr. 30, 95447 Bayreuth, Germany
E-mail: sven.huetttner@uni-bayreuth.de

Dr. A. Guerrero, Prof. J. Bisquert
Institute of Advanced Materials (INAM)
Universitat Jaume I
12006 Castellö, Spain

C. A. M. Luna, Prof. J. Köhler, Dr. R. Hildner
Experimental Physics IV and Bayreuth Institute of
Macromolecular Research
University of Bayreuth
Universitätstr. 30, 95447 Bayreuth, Germany

C. A. M. Luna
Centre for Bioinformatics and Photonics – CIBioFi
Calle 13 No. 100-00, Edificio 320 No. 1069, 760032 Cali, Colombia

C. A. M. Luna
Departamento de Fisica
Universidad del Valle
760032 Cali, Colombia

Prof. J. Bisquert
Department of Chemistry
Faculty of Science
King Abdulaziz University
21589 Jeddah, Saudi Arabia

Ultrafast spectroscopy has successfully been used to characterize the charge carrier generation/recombination process on timescales faster than nanoseconds in perovskites.[6,22] However, the contribution of ions/defects to slow dynamics with timescales of ≈10 s is still not fully elucidated.[19,23,24] In this work, correlated wide-field PL imaging microscopy[18,25] and impedance spectroscopy (IS)[26,27] serve as a powerful tool to investigate the ionic/electronic dynamic processes in perovskite films. Furthermore, we demonstrate a method, which allows to directly visualize the migration of ions within a perovskite film.

We fabricated perovskite films for PL imaging by spin-coating the mixed halide precursor solution (CH_3NH_3I:$PbCl_2$ = 3:1) on cleaned glass substrates followed by annealing at 100 °C for 1 hour in a nitrogen glovebox. These films exhibit PCEs of ≈13.5% (**Figure 1**a), when employed in standard solar cell device architectures (as shown in Figure S1, Supporting Information). Figure 1b depicts the schematic of a wide-field PL imaging microscope. A detailed description has been reported previously.[28] Briefly, we use a home-built optical microscope, and employ wide-field illumination and a charge-coupled device (CCD) camera as a detector to obtain PL images of large areas (diameter ≈60 µm) of a sample. We are able to record typically sequences of up to 2000 PL images with exposure times as short as 50 ms per image. This enables us to track the temporal/spatial evolution of the PL intensity from a perovskite film under continuous laser illumination.

Figure 1c illustrates the scanning electron microscopy (SEM) image of a perovskite film on glass, while Figure 1d is the PL image of the same film on a similar scale (yet not of the same region). The SEM image in Figure 1c shows that the perovskite film possesses densely packed grains ranging from 100 to 800 nm in size (Figure S2, Supporting Information), which is consistent with the PL image (Figure 1d). We note that on the surface of the device, the spatial distribution of the PL intensity is not uniform. This may be ascribed to the inhomogeneous distribution of composition and defects. Note that it has been reported that the presence of oxygen and moisture may result in a significant increase of the PL.[16,29] Here, to rule out the influence of ambient atmosphere, we deposited a poly(methyl methacrylate) (PMMA) layer with ≈200 nm thickness on top of the perovskite film as a protection layer. In addition, the device was in direct contact with the microscope immersion oil during the whole PL characterization.

It has been proposed that the migration/segregation of ions plays an important role for the decay of PL intensity.[15,17,19,21,30] These ions can be driven by an external electric field. Therefore, we recorded PL images as function of time on films with laterally interdigitated electrodes with channel lengths of ≈200 µm (see **Figure 2** and inset in **Figure 3**). Applying a constant electric field of ≈10^5 V m^{-1}, we observe that initially the PL intensity in the bright areas exhibits a uniform decrease as the device is connected with the external electrical circuit (Figure S4, Supporting Information). This is attributed to the charge extraction by the external electric field, which decreases the population of photogenerated charge carriers. Interestingly, under the constant electric field, a front forms that separates bright and dark domains and that moves from the positive electrode toward the negative one, as shown sequentially in Figure 2.

Note, that in the immediate vicinity on the bright side of the migrating front (Figure 2c,d, for instance), the PL intensity is exceptionally high. This may already be a hint that at this boundary an electrochemical reaction occurs (see below). Taking into account the direction of the front, from positive toward negative electrode, we assign this movement of PL dark area to the migration/accumulation of negative ions, that is, iodide ions in perovskite.[15,18] This observation is consistent with previous studies on the ionic migration, in which mainly iodide ions contribute to the hysteresis behavior[26,31–33] and field driven degradation.[34,35] As shown in Figure 2, the whole PL image (diameter is around 60 µm) is turned dark within ≈50 s under the electric field of 10^5 V m^{-1}. Therefore, the analysis of the kinetics of the migrating front enables to directly estimate the velocity of ionic migration.

To investigate this ionic motion, we characterize the velocity of the migrating front as a function of external electric field. By varying the strength of the field, we find that the migration velocity is proportional to the field within the error, as shown in Figure 3. Ignoring the ion diffusion, based on a first-order approximation, this movement of the front can be described by a simple ionic mobility theory:[36]
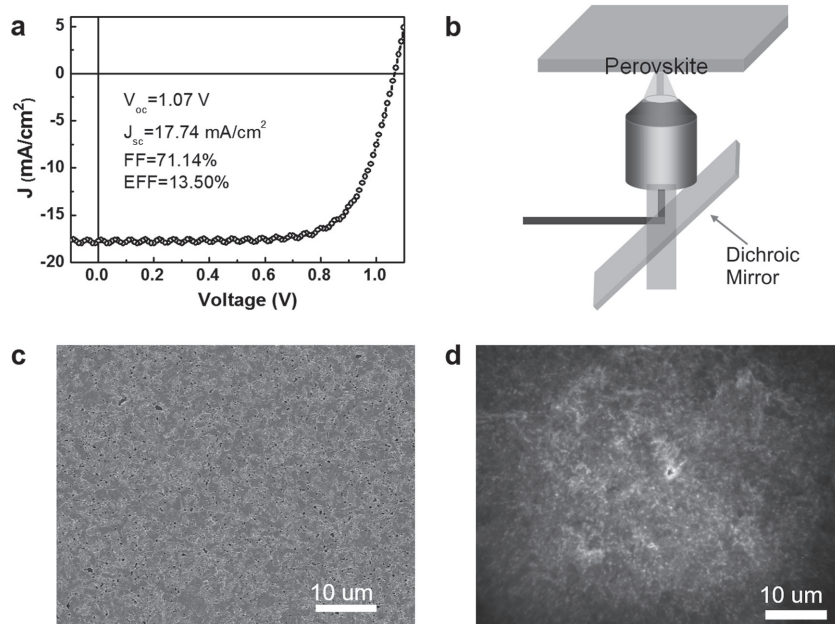
$$v = \mu E \tag{1}$$

Figure 1. a) Current density–voltage (J–V) curve of a perovskite solar cell under AM 1.5G illumination, with the structure depicted in Figure S1 (Supporting Information). b) Schematic diagram of a confocal PL imaging microscopy. c) SEM image of a perovskite film on a glass substrate. d) PL image of the perovskite film (not the same area). The excitation source is a 532 nm laser with an intensity of ≈40 mW cm^{-2}, the exposure time is 50 ms.
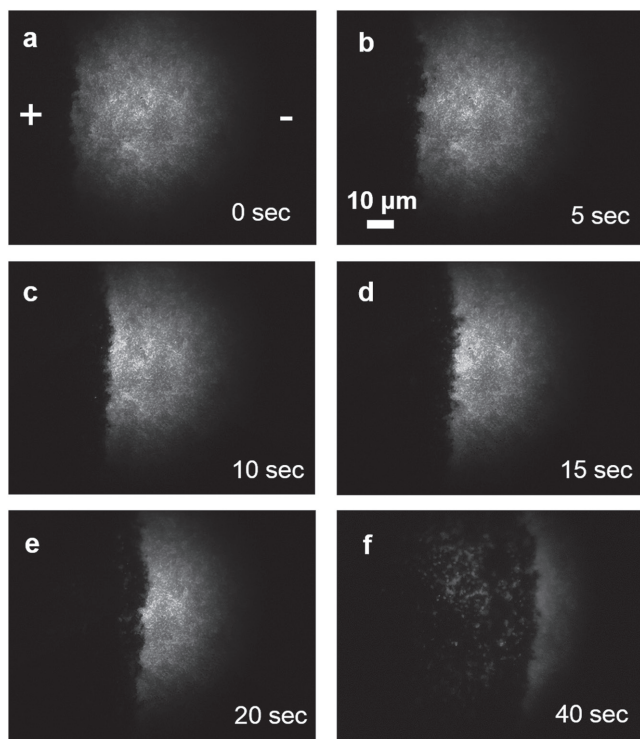
ADVANCED
SCIENCE NEWS
www.advancedsciencenews.com

NANO · MICRO
small
www.small-journal.com

Figure 2. Time dependent PL images of a perovskite film under an external electric field ($\approx 10^5$ V m^{-1}). The "+" and "−" signs indicate the polarity of the electrodes. The excitation intensity is ≈ 40 mW cm^{-2} and the exposure time per image is 50 ms. The scale bar represents 10 µm.

Here, v is the drift velocity of ion movement, μ is the mobility of ions, and E is the electric field across the whole channel. By fitting the field dependent ionic migration (two lower voltages),

the mobility of iodide ions is obtained $(5 \pm 2) \times 10^{-12}$ m^2 V^{-1} s^{-1}. This value is close to the ionic migration mobility obtained in CH$_3$NH$_3$PbI$_3$,[34,37] the discrepancy between the two values (one order of magnitude difference) may be due to the different defect densities, film fabrication processes (using PbCl$_2$ instead of PbI$_2$ as the precursor), or nature of grain boundaries. Based on the Einstein relation:[36]

$$D = \mu k_B T \qquad (2)$$

where D is the diffusion constant, k_B is Boltzmann's constant, and T is the absolute temperature, we obtain the diffusion constant D of $(1.0 \pm 0.4) \times 10^{-13}$ m^2 s^{-1}, which also agrees with the value $\approx 10^{-12}$ m^2 s^{-1}, obtained by Yang et al.[38] Here, note that the last point (1×10^5 V m^{-1}) deviates from the fitting line. This is attributed to the degradation of the perovskite film under high electric fields, consistent with the grazing incidence wide angle X-ray scattering (GIWAXS) results performed under different electric fields (Figure S5, Supporting Information).

To further understand ionic motion within the film we reversed the bias and monitored the time evolution of the dark area. We observe, that under the reversed electric field, recovery into bright areas, although with much slower speed, takes place (shown in Figure S6, Supporting Information). This asymmetry may be associated with electric field induced chemical reactions,[39] and will be further addressed below. It is also observed that after 12 hours without applied external electric field, the dark area returns to bright (not shown here). This reversible phenomenon is consistent with the iodide ion diffusion process characterized in previous papers.[18,31]

The laser power has been optimized for fast acquisition and as low as possible introduced power. We note, that the laser excitation power may play an important role in PL quantum efficiency[12] and dynamics.[30,40] Wang et al.,[41] for example, found a photo-driven transformation in CsPbX$_3$ nanostructures. Xing et al.[42] observed a decreased activation energy for ion migration under light illumination and the presence of migrating ions has direct implications on slow dynamic optical processes in perovskite-based devices as has been recently reviewed by Panzer et al.[40]

IS has been demonstrated to be a powerful tool to explore the microscopic processes in perovskite solar cells, especially the migration of ionic charges.[27,39,43] In this work, we carried out IS measurements with the aim to electrically monitor how ions are piling up at one electrode and to correlate with the PL measurements by performing both measurements quasi-simultaneously. In a typical IS measurement a DC bias is applied to polarize the sample and a small AC perturbation is superimposed. As we have seen, ionic concentration shifts as a function of time showing a constant mobility. Therefore, the combination of the two methods allows us to implement this additional parameter in the interpretation of the IS results. The differential current output is measured, which offers information on the capacitive and resistive processes taking place in an operating device. For perovskite devices it has previously been demonstrated that the response in the low frequency region is related to electrode polarization of ions by generation of a Helmholtz layer and charge compensation by the external electrode.[43]
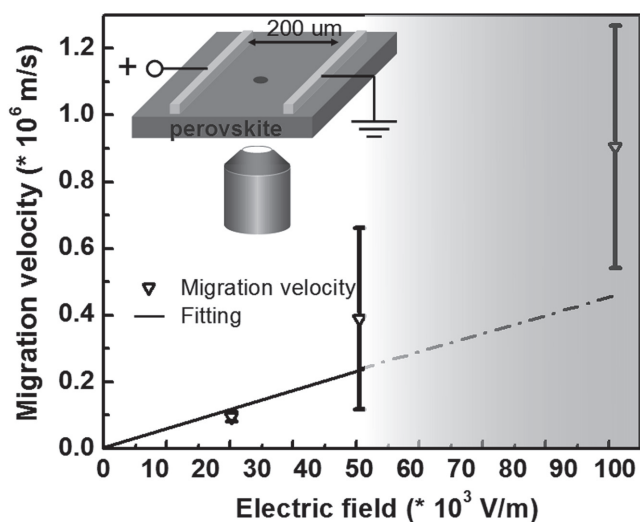

Figure 3. Field dependence of the ionic migration velocity. Inset: the schematic diagram of the setup. The black line is the fitting line based on first two points (lower voltages) considering the weight of error. Dashed line is the extension of the fitting line, because at high voltage, the perovskite film exhibits decomposition (see Figure S5, Supporting Information). The gradient color indicates the more chemical decomposition under higher voltage.

**ADVANCED
SCIENCE NEWS**
www.advancedsciencenews.com
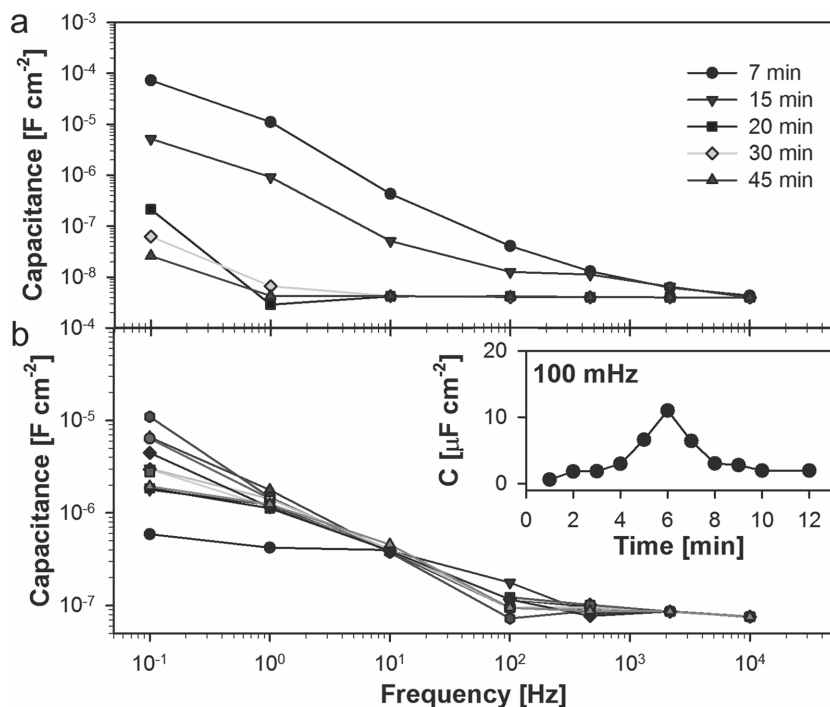
NANO · MICRO
small
www.small-journal.com

Figure 4. Capacitance–frequency plot of IS measurements carried out simultaneously during PL measurement by applying a DC bias of a) 1 V and b) 2 V. The inset shows the evolution of the capacitance at 100 mHz with time.

As shown in **Figure 4**a, initially a DC bias of 1 V was applied in the dark to induce ion migration toward the electrodes by using a potentiostat equipped with a frequency analyzer, which is able to acquire impedance spectroscopy in situ. The PL image was recorded at every end of each IS cycle (PL images shown in Figure S7, Supporting Information). It is important to note that under this very mild field of only 1 V applied between the contacts no noticeable advance front is observed in Figure S7 in the Supporting Information, though as established above (Figure 3) we can assume a constant mobility. Hence, a lower voltage gives us sufficient time to carry out the respective IS cycles. Furthermore, IS measurements are very sensitive to changes at the interface level between perovskite layer and contacts. Indeed, Figure 4a shows the capacitance–frequency plot as a function of time. After the first IS measurement scan (7 min) the capacitance at low frequencies (0.1 Hz) is initially in the range of ≈70 µF cm^{-2}, which is a typical capacitance value produced from piling up ions at one interface due to electrode polarization.[43] Interestingly, as the polarization time increases, this low frequency capacitance decreases with lowest value observed (20 nF cm^{-2}) after 45 min of applied bias which could be the result of an electrochemical reaction leading to the generation of neutral species (i.e., PbI$_2$).[34] PbI$_2$ is neutral and as such will not give rise to a capacitive response, for this reason the capacitance will reduce with time as the material forms. The detailed electrochemical reaction will be addressed in the following part.

Subsequently, IS measurements were carried out with a polarization of 2 V (Figure 4b) with a shorter delay time (1 min). These conditions allow monitoring how the ions

accumulate at one interface as a function of the time and the electrochemical reaction leading to neutral species at the electrode. Initially, the capacitance in the low frequency region is low as no ions are present in the interface (≈0.7 µF cm^{-2}) and this increases with the time to reach a maximum capacitance value (10 µF cm^{-2}) observed at 6 min indicating that after this time most of the electrode surface is covered by charged ions that have migrated from the bulk of the perovskite layer. Note that capacitances are not as high as in the previous experiment as some of the interfacial area has already reacted in the previous experiment leading to inactive areas. After this time the capacitance begins to decrease as shown in the inset of Figure 4b similar to the effect observed for polarization at 1 V. Capacitances of ≈2 µF cm^{-2} are observed after 12 min of polarization indicating that the charged species covering the electrode have mostly reacted to generate neutral species.

A different set of measurements, with the same device structure, was carried out where the capacitance was measured as a function of the applied bias (**Figure 5**a) in the dark. In this set of experiments, the frequency range was increased to cover still lower frequencies (down to 5 mHz). As expected noise increases in this region as a consequence of the slow response of mobile ions to the small AC perturbation. The electrode polarization capacitance increases with the applied bias exponentially.

The observation of a variation of the capacitance with voltage, shown in Figure 5b, is a clear indication of charge accumulation at the interface. A number of previous studies have clearly shown that the large low frequency capacitance of perovskite solar cells in the dark can originate from the mobile ion accumulation.[43,44] In principle, if the ions move freely in the solid medium the structure of the interface consists of a double layer and a diffuse layer that is controlled by the applied voltage. For a symmetric electrolyte the Gouy–Chapman model gives the capacitance:[45]

$$C = \frac{\varepsilon \varepsilon_0}{L_D} \sin h\left(\frac{qV}{2k_B T}\right) \tag{3}$$

where V is the potential drop between the metallic contact and the absorber bulk, ε_0 is the permittivity of vacuum, ε is the dielectric constant of perovskite, and $k_B T$ is the thermal energy, q is the charge. The ion Debye length L_D is therefore given by:

$$L_D = \sqrt{\frac{\varepsilon \varepsilon_0 k_B T}{q^2 N}} \tag{4}$$

Here N accounts for the equilibrium density of ionic charges in the bulk material. Equation (3) indicates that the extension of disequilibrium of ionic distribution at the interface is of size L_D. The capacitance at zero bias is:

**ADVANCED
SCIENCE NEWS**
www.advancedsciencenews.com
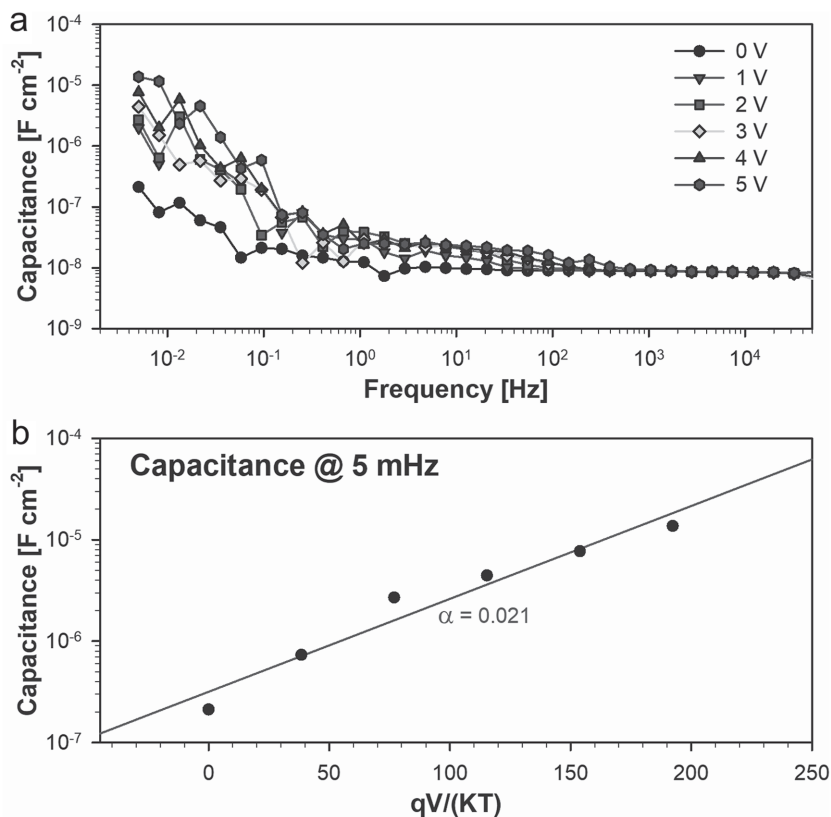
NANO MICRO

small
www.small-journal.com

Figure 5. a) Capacitance–frequency plot of measurements carried out in the dark as a function of the applied bias. b) Exponential relationship of capacitance as a function of external voltage measured at 5 mHz. α accounts for the exponential distribution of states characterized by a temperature parameter T_0 as $\alpha = T/T_0$.

$$C_1 = \frac{\varepsilon \varepsilon_0}{L_D} \qquad (5)$$

The thermalized distribution of ions in Equation (3) can be approximated by the formula:

$$C = C_0 e^{\frac{\alpha q V}{k_B T}} \qquad (6)$$

With $C_0 = C_1$ and a parameter $\alpha = 1/2$ that correspond to the thermalized accumulation of freely diffusing ions according to their electrochemical potential. However, the experimental observations reported in Figure 5 show that $\alpha = 1/2$ is far from being satisfied. Since $\alpha \approx 0.02$, as shown in Figure 5b, it is apparent that the rise of capacitance does not correspond simply to the thermalized distribution of ions, but to an exponential distribution of states characterized by a temperature parameter T_0 as $\alpha = T/T_0$.[46] This exponential distribution of states is a common occurrence in ionic and electronic systems that are characterized by a large degree of disorder. For example, a distribution of states has been observed in the intercalation of Li+ ions into WO_3 electrochromic thin films[47] and also for the insertion of Li into ultrathin Ge layer in Si/Ge battery cathodes.[48]

The observation of an exponential density of states for the accumulation of ions close to the perovskite/Au electrode
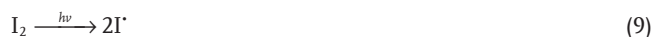
interface indicates that ions become immobilized in the host material with the given distribution. According to the observation of the large changes of capacitance reported above, we can assume that such a distribution is not intrinsically formed at the interface but rather has been caused by the prolonged voltage applied to the symmetric cell. Therefore, a special layer is formed at the interface, which is richer in I_2 and reduces the ability to take ions from the bulk. Tentatively, we assume that reaction at the metal surface produces a film of PbI_2 that contains the exponential distribution suggested in Equation (6). This observation would be consistent with the formation of a PbI_2 layer under a continuous electrical bias, and the electrochemical reaction is proposed as:[34]

$$MAPbI_3 \rightarrow PbI_2 + MA^+ + I^- \qquad (7)$$

$$2I^- \rightarrow I_2 \uparrow + 2e^- \qquad (8)$$
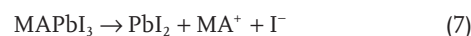
In addition, Li et al.[31] observed that after long term biasing at the positive electrode, the ratio between iodine and lead is away from the stoichiometric ratio of perovskite, suggesting the formation of PbI_2. Furthermore, Figure S5 of the Supporting Information indicates that there exists PbI_2 signal after electrical biasing characterized by GIWAXS measurement. Deng et al.[18] also obtain the PbI_2 signal by investigating the PL signal near the positive electrode.

To further understand the role of iodide ions on the PL performance of devices, we recorded time dependent PL spectra under an iodine vapor atmosphere with the configuration displayed in **Figure 6**a. As shown in Figure 6b, as the I_2 vapor (mixed with N_2 gas flow) was introduced into the chamber, the PL intensity immediately decreases. After 30 s, the PL intensity decreased by around two orders magnitude. Then the I_2 saturated gas was turned off and the chamber was purged with pure N_2 leading to a recovery of the PL intensity to its original value after ≈5 min. The optical absorption of iodide vapor[49] does not affect the excitation (532 nm) or the emission signal (≈780 nm) (Figure S9, Supporting Information). This PL quenching is only associated with the influence of iodine doping in the perovskite film. Wang et al.[50] proposed the chemical reaction of perovskite materials exposure to the high concentration of iodine vapor. The proposed chemical reaction reads as:
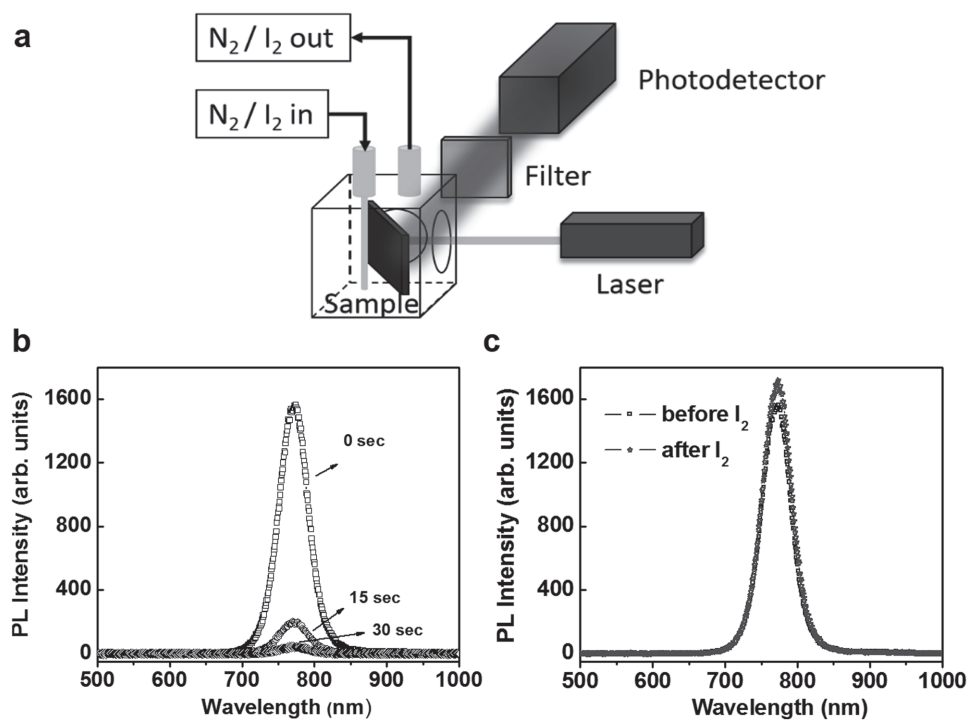
(i) under visible or ultraviolet light

$$I_2 \xrightarrow{h\nu} 2I^{\bullet} \qquad (9)$$

$$2I^- + 2I^{\bullet} \xrightarrow{h\nu} 2I_2^{-} \qquad (10)$$

ADVANCED
SCIENCE NEWS
www.advancedsciencenews.com

NANO MICRO
small
www.small-journal.com

Figure 6. a) Schematic diagram of the PL quenching/recovery experiment using I_2 saturated N_2 and pure N_2 vapor, respectively. The excitation source is a laser with wavelength of 532 nm. b) Temporal evolution of the PL intensity of a perovskite film in I_2 vapor. PL spectra were recorded every 3 s. c) Recovery of PL intensity of perovskite film after 5 min in a pure N_2 atmosphere.

With assistance of light, atomic iodine ($I^•$) is generated in the iodine vapor based on Equation (9). Then these atomic iodines can react with iodide ions (I^-), forming $I_2^{•-}$ based on Equation (10). $I_2^{•-}$ can further react with MA^+ ions, leading to the degradation of perovskite materials.

(ii) under darkness

$$I^- + I_2 \rightleftarrows I_3^-$$ (11)

According to Equation (11), triiodide ions (I_3^-) are formed in the iodine vapor. I_3^- can further participate the following reaction with MA^+ ions. Both of the above reactions will lead to the degradation of perovskite, forming CH_3NH_2 gas and PbI_2. Here, note that, in this work, under relatively low concentration iodine vapor, the reversible change of PL intensity suggests the reversible chemical reaction, rather than irreversible structure degradation.[18] Currently, the detailed microscopic process is still under investigation, however this rather simple experiment elucidates the direct and reversible influence of accumulated iodide.

Now, we can provide a picture on the evolution of PL dark areas on the perovskite film under external electric fields. This enhanced nonradiative recombination pathway includes both the trap-assisted recombination[51] and possible Auger-like recombination due to the charged mobile defects.[18,21] Under external fields, as shown in **Figure 7**, the mobile ions obtain sufficient energy to overcome the activation energy[33,52] and start to drift. These accumulated charges enhance the local electric field.[15] It is known that the excited states are significantly

influenced by its surrounding, e.g., ionized grains,[53] which results in the PL quenching.[21,54] By employing time-of-flight secondary-ion-mass spectrometry with PL microscopy, de Quilettes et al.[55] find that excess iodide ions are driven by an optical field away from the illuminated region. Subsequently, this redistribution of iodide ions gives rise to the rising of PL intensity under continues light illumination by decreasing the local iodide ion concentration. Nevertheless, how the excess iodide ions contribute to the nonradiative recombination is still not fully elucidated. Iodide interstitials,[56] acting as shallow defects, should not lead to significant charge recombination. Agiorgousis et al.[57] suggest that both lead dimers and iodide trimers may form with strong covalent bonds at defects, performing as

Figure 7. Schematic diagram of the influence of iodide ion migration on the PL intensity under an external electric field. The electric field drives the ions, leading to the accumulation of these ions which enhance the nonradiative recombination in these individual grains. These grain boundaries serve as the main pathways for the ionic migration.

ADVANCED
SCIENCE NEWS
www.advancedsciencenews.com

NANO · MICRO
small
www.small-journal.com

strong covalency-induced recombination centers. The detailed understanding, however, is still under investigation.

Here, it is necessary to mention that during this experiment, we cannot completely rule out the migration or reorientation of MA$^+$ ions under an electric field,[17,58] though the recent evidences in the literature point toward iodine. Previous works proposed that the migration of MA$^+$ ions and Pb vacancies may play a role in the hysteresis of perovskite solar cells.[26,37] However, Eames et al.[32] estimated that the diffusion coefficient of MA$^+$ ions is four orders of magnitude lower than the one of iodide ions. In addition, the direct observation of accumulation of negative ions at the positive side suggests the main contribution of halide ions rather than other defects.[15,31] This may be attributed to the low mobility and higher activation energy for other defects, e.g., Pb vacancies, MA$^+$ ions, etc.[59] In this work, we observed the migration of ions in relatively low electric field ($\approx 10^5$ V m^{-1}), so the phase change should also not be the main reason.

The exact ionic migration pathway is still unclear. Due to the large density of defect states in the perovskite film, ascribed to the low-temperature film fabrication, the defect facilitated ion migration may play an important role. Beside moving through bulk point defects, more and more evidence indicates that the grain boundary, where large amount of defects exist due to the lack of perfect crystalline structure, serves as the main ionic migration channel.[23,60] Due to the loss of the half chemical bond at grain boundary, these defects, e.g., iodide vacancies or iodide interstitials sites, facilitate the ionic migration through defect site replacing.[23] In addition, at temperature 330 K under external electric field, decomposed PbI$_2$ thread was observed, migrating along external field.[34] Therefore, field-induced structure decomposition/distortion may also play a role in ionic migration.

Video in the Supporting Information demonstrates the movement of PL inactive area is in the form of migration through grain by grain. This suggests that under external electric field, with the assistance of grain boundaries, iodide ions drift toward and accumulate at the positive electrode. When the concentration of iodide ion reaches a certain threshold, PL quenching is observed. By investigating the ion migration properties in perovskite films and single crystal, Xing et al.[42] found that the activation energy of ions strongly depends on the size of grain. In addition, the research on the grain size dependence of ionic migration, characterized by PL microscopy is processing in our group. However, this is beyond the scope of this paper.

In addition, a different case is observed when the ion does not act merely as a spectator but lead to chemical reactions with the surrounding materials. Obviously, in this case the rate of the reactions may be limited by the ions supply and this will follow diffusive limitations. In the case of perovskite solar cells, it looks like we are able to remove 1–3 iodide ions from each unit cell according to previous results.[61]

It is necessary to mention that the moving front in Figure 2 might not be actually ions migration but the reaction product between the perovskite and the excess ions. In fact, this impressive flat profile of the fronts as shown in Figure 2 is not usually observed in diffusive processes and rather implies that a certain threshold value of accumulated iodine is responsible for this phenomenon. In addition, it is noted that the velocity of moving front across the whole channel is not a constant, suggesting an ionic space charge effect. The detailed process is under investigation.

Beside in perovskite solar cells, ion migration also plays an important role in perovskite light emitting diodes (LEDs) and the herein presented experiments can help to shine light into respectively observed dynamics. For instance, in typical perovskite LEDs,[62] considering a dielectric constant of CsPbX$_3$ quantum dots ($\varepsilon_r \approx 5$)[63] and polymer transport layer ($\varepsilon_r \approx 3$), the electric field dropped on this perovskite layer is in the order of 10^7 V m^{-1}. These fields are even larger than the once applied in this experiment (Figure 3), which renders even faster migration velocities. For example, Tan et al.[11] observed respective time dependent performance and hysteresis behavior. The timescale of increases in external quantum efficiency of the LEDs under pulsed voltage is less than 0.01 s.

In conclusion, we demonstrate a direct method to visualize ion migration in an electric field in organolead halide perovskite films through wide-field PL imaging microscopy. It is evident that local stoichiometric variations due to external electric field have a significant impact on the local PL performance, and therefore influence the solar cells performance. This field-driven inhomogeneity is associated with the iodide ions migration, which is confirmed by both the IS characterization and PL quenching under I$_2$ vapor. By employing PL imaging microscopy in combination with IS, we further characterize dynamic process of these iodide ions when monitoring the migration of PL inactive area under an external electric field in a lateral-configured electrode device. Hence, wide-field PL imaging microscopy provides an in situ approach to investigate the ionic migration, which has an obvious impact on the photovoltaic performance, such as J–V hysteresis and chemical degradation. This provides a powerful tool to investigate the influence of grain boundaries, crystal size, or passivation procedures in perovskite thin films. To further improve the performance and stability of perovskite solar cells, it is important to carefully control the defect/ions migration within the operating device, either by decreasing the defect density in the bulk (crystalline size and quality) or alleviating the long-term biasing effect in the vicinity of electrodes.

Experimental Section

Perovskite Solar Cells Device Fabrication and Characterization: CH$_3$NH$_3$I (MAI) was purchased from Tokyo Chemical Industry company, and Spiro-OMeTAD (2,2′,7,7′-Tetrakis-(*N*,*N*-di-4-methoxyphenylamino)-9,9′-spirobifluorene) was purchased from Merck company. All the other chemicals were purchased from Sigma-Aldrich and were used as received.

Fluorine-doped tin oxide (F:SnO$_2$) (FTO) transparent conducting glasses were cut and patterned by Zn power and HCl solution. FTO glasses were washed with acetone, 2% hellmanex diluted in deionized water and isopropanol successively for 10 min each. Then by spraying a solution of titanium diisopropoxide bis(acetylacetonate) (0.6 mL) in ethanol (21.4 mL) at 450 °C for 90 min in ambient atmosphere, a compact TiO$_2$ layer ($\approx$50 nm) was deposited.

MAI and lead chloride (PbCl$_2$) (3:1 molar ratio) were dissolved in anhydrous *N*,*N*-dimethylformamide. Then, this precursor solution was spin-coated on the TiO$_2$/FTO substrates at 3000 rpm for 60 s. After drying for $\approx$30 min, the as-spun films were annealed at 100 °C for 90 min. Following that, Spiro-OMeTAD solution was prepared by dissolving 72.3 mg Spiro-OMeTAD, 26.3 µL lithium-bis(trifluoromethanesulfonyl)imide (Li-TFSI) solution (520 mg Li-TFSI in 1 mL acetonitrile), and 43.2 µL 4-tert-butylpyridine in 1 mL chlorobenzene. This hole transport

layer was deposited by spin-coating at 4000 rpm for 30 s. All device fabrication steps were carried out within a nitrogen gas filled glovebox. The whole of the device was exposed in a dry box (ambient atmosphere with humidity <5%) for more than 12 h. Finally, a 150 nm silver electrode was deposited by thermal evaporation in a chamber with a pressure of $\approx 1 \times 10^{-6}$ mbar. The effective electrode area was 9 or 16 mm^2.

J–V measurements were performed under inert environment with a Keithley 2400 source measure unit under 100 mW cm^{-2} illumination from an AM 1.5 solar simulator. The active area of 4 and 9 mm^2 was defined by the overlap of a black mask aperture area, the FTO, and the evaporated top electrode. The light intensity was calibrated before by a silicon detector. There was no prebiasing process. The scanning speed was 0.9 V s^{-1}.

Perovskite Film Fabrication for PL Imaging Experiment: The similar procedure was used to fabricate the film for the PL imaging characterization. Glass substrates were washed with acetone, and isopropanol successively for 10 min each. Then these glass substrates were treated with Ozone for around 10 min. Following that, in a nitrogen glovebox, perovskite precursor was spin-coated on glass substrates at 3000 rpm for 60 s. These as-spun films were subsequently annealed at 100 °C for 60 min in the glovebox. In the end, a 40 mg mL^{-1} PMMA solution dissolved in butyl acetate (anhydrous, 99%) was then spin-coated on the perovskite film as a protection layer, at speed of 2000 rpm for 60 s.

For the PL imaging experiments under electric field, perovskite films on glass were transferred into an evaporation chamber with pressure of 1×10^{-6} mbar, and ≈ 100 nm thickness of gold was deposited by thermal evaporation through a shadow mask. The electrode distance was 200 μm and the interdigitating electrode geometry provided a ratio between channel width *W* and length *L*, *W/L* of 500.

PL Imaging Experiment: The setup used for PL imaging of perovskite films was based on a home-built confocal microscope. The specimen was illuminated by a laser with wavelength of either 450 or 532 nm (LDH-C-450B or LDH-P-FA 530L, 20 MHz repetition rate, 70 ps pulse duration, Picoquant), resulting in excitation of free charge carriers.

The excitation power can be controlled by neutral density attenuation filters and was set to ≈ 40 mW cm^{-2} in the sample plane. The laser light was spatially filtered and directed to the microscope, which was equipped with an infinity-corrected high-numerical-aperture oil-immersion objective (60×, numerical aperture of 1.45, Olympus). The perovskite film was placed in the focal plane of the objective lens, and the sample position was controlled by a piezostage (Tritor 102 SG, from piezosystem Jena). An additional lens (wide-field lens) was flipped into the excitation beam path to focus the laser light into the back focal plane of the microscope objective. This allowed for illumination of a large area with ≈ 60 μm diameter in the sample plane.

The PL signal was collected by the same objective, passed a long-pass filter (LP 467 or LP545, AHF) to suppress residual laser light, and was imaged onto a CCD camera (Orca-ER, Hamamatsu). For electric field dependent measurement (see Video in the Supporting Information), the PL was recorded with a constant 20 V DC voltage being applied between the Au electrodes.

Impedance Spectroscopy: The setup to measure impedance spectroscopy is similar to that described previously for PL analysis. However, in this case the DC voltage source to polarize the sample was a potentiostat equipped with a frequency analyzer (Zahner Potentiostat, Zenium). A small AC perturbation was applied and the differential current output was measured to calculate the impedance response. The frequency window was kept small ranging between 10 kHz and 100 mHz to minimize the measurement time. Each frequency scan took less than 1 min and a delay time of 5 min was used between scans to carry out the PL measurements. The light source was turned off after the PL measurement and the new IS scan was taken under dark conditions. For measurements at a DC voltage of 2 V the delay time was reduced to 30 s and this enabled the observation of the accumulation of ions at the interface. Alternatively, devices were measured systematically under a range of applied bias using a high sensitivity potentiostat (Autolab PGSTAT-30) to cover a lower frequency ranged down to 5 mHz.

PL under Iodine Atmosphere: The PL of a perovskite film was measured under iodine atmosphere. For this, a perovskite film was placed in an atmospherically sealed measuring chamber with quartz glass windows. Before starting the measurement, the chamber was heated to roughly 50 °C using a heat gun in order to prevent condensation of solid iodine onto the windows and the perovskite film. The photoluminescence measurements under iodine were performed using an 80 mW laser (PGL V – II) with a wavelength of 532 nm. The spectra were recorded using a spectrometer (QE Pro from Ocean Optics) and matching optical fiber. A filter (OG 590 nm) was used to filter the emission light.

Initially, the PL was measured under a pure nitrogen atmosphere to obtain a reference value. Subsequently, a vial with solid iodine was connected to the gas inlet pipeline and thus the chamber was filled with a mixed iodine/nitrogen atmosphere. Upon connecting the iodine vapor, a PL spectrum was measured every 3 s to observe the progress of the PL intensity. After the PL intensity stabilized on a lower level, the iodine was disconnected from the gas pipeline and flushed the measurement chamber with pure nitrogen.

Supporting Information

Supporting Information is available from the Wiley Online Library or from the author.

Acknowledgements

Conflict of Interest

The authors declare no conflict of interest.

Keywords

[1] A. Kojima, K. Teshima, Y. Shirai, T. Miyasaka, *J. Am. Chem. Soc.* **2009**, *131*, 6050.

[2] W. S. Yang, J. H. Noh, N. J. Jeon, Y. C. Kim, S. Ryu, J. Seo, S. I. Seok, *Science* **2015**, *348*, 1234.

[3] a) T. C. Sum, N. Mathews, *Energy Environ. Sci.* **2014**, *7*, 2518; b) Y.-C. Hsiao, T. Wu, M. Li, Q. Liu, W. Qin, B. Hu, *J. Mater. Chem. A* **2015**, *3*, 15372.

[4] S. D. Stranks, H. J. Snaith, *Nat. Nanotechnol.* **2015**, *10*, 391.

ADVANCED
SCIENCE NEWS
www.advancedsciencenews.com

NANO · MICRO
small
www.small-journal.com

[5] a) K. Tvingstedt, O. Malinkiewicz, A. Baumann, C. Deibel, H. J. Snaith, V. Dyakonov, H. J. Bolink, *Sci. Rep.* **2014**, *4*, 6071; b) A. Filippetti, P. Delugas, A. Mattoni, *J. Phys. Chem. C* **2014**, *118*, 24843; c) W. E. I. Sha, X. Ren, L. Chen, W. C. H. Choy, *Appl. Phys. Lett.* **2015**, *106*, 221104; d) W. Tress, N. Marinova, O. Inganäs, M. K. Nazeeruddin, S. M. Zakeeruddin, M. Graetzel, *Adv. Energy Mater.* **2015**, *5*, 1400812.

[6] Y. Yamada, T. Nakamura, M. Endo, A. Wakamiya, Y. Kanemitsu, *J. Am. Chem. Soc.* **2014**, *136*, 11610.

[7] L. M. Herz, *Annu. Rev. Phys. Chem.* **2015**, *67*, 65.

[8] N. K. Noel, A. Abate, S. D. Stranks, E. S. Parrott, V. M. Burlakov, A. Goriely, H. J. Snaith, *ACS Nano* **2014**, *8*, 9815.

[9] W. Shockley, H. J. Queisser, *J. Appl. Phys.* **1961**, *32*, 510.

[10] O. D. Miller, E. Yablonovitch, S. R. Kurtz, *IEEE J. Photovoltaics* **2012**, *2*, 303.

[11] Z.-K. Tan, R. S. Moghaddam, M. L. Lai, P. Docampo, R. Higler, F. Deschler, M. Price, A. Sadhanala, L. M. Pazos, D. Credgington, F. Hanusch, T. Bein, H. J. Snaith, R. H. Friend, *Nat. Nanotechnol.* **2014**, *9*, 687.

[12] J. Wang, N. Wang, Y. Jin, J. Si, Z.-K. Tan, H. Du, L. Cheng, X. Dai, S. Bai, H. He, Z. Ye, M. L. Lai, R. H. Friend, W. Huang, *Adv. Mater.* **2015**, *27*, 2311.

[13] F. Deschler, M. Price, S. Pathak, L. E. Klintberg, D.-D. Jarausch, R. Higler, S. Hüttner, T. Leijtens, S. D. Stranks, H. J. Snaith, M. Atatüre, R. T. Phillips, R. H. Friend, *J. Phys. Chem. Lett.* **2014**, *5*, 1421.

[14] D. W. de Quilettes, S. M. Vorpahl, S. D. Stranks, H. Nagaoka, G. E. Eperon, M. E. Ziffer, H. J. Snaith, D. S. Ginger, *Science* **2015**, *348*, 683.

[15] S. Chen, X. Wen, R. Sheng, S. Huang, X. Deng, M. A. Green, A. Ho-Baillie, *ACS Appl. Mater. Interfaces* **2016**, *8*, 5351.

[16] J. F. Galisteo-López, M. Anaya, M. E. Calvo, H. Míguez, *J. Phys. Chem. Lett.* **2015**, *6*, 2200.

[17] R. Gottesman, L. Gouda, B. S. Kalanoor, E. Haltzi, S. Tirosh, E. Rosh-Hodesh, Y. Tischler, A. Zaban, C. Quarti, E. Mosconi, F. De Angelis, *J. Phys. Chem. Lett.* **2015**, *6*, 2332.

[18] X. Deng, X. Wen, C. F. J. Lau, T. Young, J. Yun, M. A. Green, S. Huang, A. W. Y. Ho-Baillie, *J. Mater. Chem. C* **2016**, *4*, 9060.

[19] D. L. Jacobs, M. A. Scarpulla, C. Wang, B. R. Bunes, L. Zang, *J. Phys. Chem. C* **2016**, *120*, 7893.

[20] Y. Lin, L. Shen, J. Dai, Y. Deng, Y. Wu, Y. Bai, X. Zheng, J. Wang, Y. Fang, H. Wei, W. Ma, X. C. Zeng, X. Zhan, J. Huang, *Adv. Mater.* **2017**, *29*, 1604545.

[21] X. Wen, A. Ho-Baillie, S. Huang, R. Sheng, S. Chen, H.-c. Ko, M. A. Green, *Nano Lett.* **2015**, *15*, 4644.

[22] S. D. Stranks, G. E. Eperon, G. Grancini, C. Menelaou, M. J. P. Alcocer, T. Leijtens, L. M. Herz, A. Petrozza, H. J. Snaith, *Science* **2013**, *342*, 341.

[23] Y. Yuan, J. Huang, *Acc. Chem. Res.* **2016**, *49*, 286.

[24] S. Ravishankar, O. Almora, C. Echeverría-Arrondo, E. Ghahremanirad, C. Aranda, A. Guerrero, F. Fabregat-Santiago, A. Zaban, G. Garcia-Belmonte, J. Bisquert, *J. Phys. Chem. Lett.* **2017**, *8*, 915.

[25] a) Z. Hameiri, A. Mahboubi Soufiani, M. K. Juhl, L. Jiang, F. Huang, Y.-B. Cheng, H. Kampwerth, J. W. Weber, M. A. Green, T. Trupke, *Prog. Photovoltaic: Res. Appl.* **2015**, *23*, 1697; b) A. M. Soufiani, Z. Hameiri, S. Meyer, S. Lim, M. J. Y. Tayebjee, J. S. Yun, A. Ho-Baillie, G. J. Conibeer, L. Spiccia, M. A. Green, *Adv. Energy Mater.* **2016**, *7*, 1602111.

[26] J. M. Azpiroz, E. Mosconi, J. Bisquert, F. De Angelis, *Energy Environ. Sci.* **2015**, *8*, 2118.

[27] B. Chen, M. Yang, X. Zheng, C. Wu, W. Li, Y. Yan, J. Bisquert, G. Garcia-Belmonte, K. Zhu, S. Priya, *J. Phys. Chem. Lett.* **2015**, *6*, 4693.

[28] a) A. T. Haedler, K. Kreger, A. Issac, B. Wittmann, M. Kivala, N. Hammer, J. Kohler, H.-W. Schmidt, R. Hildner, *Nature* **2015**, *523*, 196; b) A. Issac, R. Hildner, C. Hippius, F. Würthner, J. Köhler, *ACS Nano* **2014**, *8*, 1708; c) C. Li, Y. Zhong, C. Luna, T. Unger, K. Deichsel, A. Gräser, J. Köhler, A. Köhler, R. Hildner, S. Huettner, *Molecules* **2016**, *21*, 1081.

[29] a) Y. Tian, M. Peter, E. Unger, M. Abdellah, K. Zheng, T. Pullerits, A. Yartsev, V. Sundstrom, I. G. Scheblykin, *Phys. Chem. Chem. Phys.* **2015**, *17*, 24978; b) H.-H. Fang, F. Wang, S. Adjokatse, N. Zhao, M. A. Loi, *Adv. Funct. Mater.* **2016**, *26*, 4653.

[30] R. Gottesman, A. Zaban, *Acc. Chem. Res* **2016**, *49*, 320.

[31] C. Li, S. Tscheuschner, F. Paulus, P. E. Hopkinson, J. Kießling, A. Köhler, Y. Vaynzof, S. Huettner, *Adv. Mater.* **2016**, *28*, 2446.

[32] C. Eames, J. M. Frost, P. R. F. Barnes, B. C. O'Regan, A. Walsh, M. S. Islam, *Nat. Commun.* **2015**, *6*, 7497.

[33] S. Meloni, T. Moehl, W. Tress, M. Franckevicius, M. Saliba, Y. H. Lee, P. Gao, M. K. Nazeeruddin, S. M. Zakeeruddin, U. Rothlisberger, M. Graetzel, *Nat. Commun.* **2016**, *7*, 10334.

[34] Y. Yuan, Q. Wang, Y. Shao, H. Lu, T. Li, A. Gruverman, J. Huang, *Adv. Energy Mater.* **2016**, *6*, 1501803.

[35] Z. Xiao, Y. Yuan, Y. Shao, Q. Wang, Q. Dong, C. Bi, P. Sharma, A. Gruverman, J. Huang, *Nat. Mater.* **2015**, *14*, 193.

[36] S. M. Sze, *Physics of Semiconductor Devices*, Wiley, New York, USA **1981**.

[37] Y. Yuan, J. Chae, Y. Shao, Q. Wang, Z. Xiao, A. Centrone, J. Huang, *Adv. Energy Mater.* **2015**, *5*, 1500615.

[38] T.-Y. Yang, G. Gregori, N. Pellet, M. Grätzel, J. Maier, *Angew. Chem. Int. Ed.* **2015**, *54*, 7905.

[39] J. Carrillo, A. Guerrero, S. Rahimnejad, O. Almora, I. Zarazua, E. Mas-Marza, J. Bisquert, G. Garcia-Belmonte, *Adv. Energy Mater.* **2016**, *6*, 1502246.

[40] F. Panzer, C. Li, T. Meier, A. Köhler, S. Huettner, *Adv. Energy Mater.* **2017**, *7*, 1700286.

[41] Y. Wang, X. Li, S. Sreejith, F. Cao, Z. Wang, M. C. Stuparu, H. Zeng, H. Sun, *Adv. Mater.* **2016**, *28*, 10637.

[42] J. Xing, Q. Wang, Q. Dong, Y. Yuan, Y. Fang, J. Huang, *Phys. Chem. Chem. Phys.* **2016**, *18*, 30484.

[43] O. Almora, A. Guerrero, G. Garcia-Belmonte, *Appl. Phys. Lett.* **2016**, *108*, 043903.

[44] R. S. Sanchez, V. Gonzalez-Pedro, J.-W. Lee, N.-G. Park, Y. S. Kang, I. Mora-Sero, J. Bisquert, *J. Phys. Chem. Lett.* **2014**, *5*, 2357.

[45] K. B. Oldham, *J. Electroanal. Chem.* **2008**, *613*, 131.

[46] J. Bisquert, *Nanostructured Energy Devices: Equilibrium Concepts and Kinetics*, CRC Press, Boca Raton, FL **2014**.

[47] M. Strømme Mattsson, *Phys. Rev. B* **1998**, *58*, 11015.

[48] M. Haro, T. Song, A. Guerrero, L. Bertoluzzi, J. Bisquert, U. Paik, G. Garcia-Belmonte, *Phys. Chem. Chem. Phys.* **2014**, *16*, 17930.

[49] S. George, N. Krishnamurthy, *Am. J. Phys.* **1989**, *57*, 850.

[50] S. Wang, Y. Jiang, E. J. Juarez-Perez, L. K. Ono, Y. Qi, *Nat. Energy* **2016**, *2*, 16195.

[51] G.-J. A. H. Wetzelaer, M. Scheepers, A. M. Sempere, C. Momblona, J. Ávila, H. J. Bolink, *Adv. Mater.* **2015**, *27*, 1837.

[52] H. Yu, H. Lu, F. Xie, S. Zhou, N. Zhao, *Adv. Funct. Mater.* **2016**, *26*, 1411.

[53] P. Anger, P. Bharadwaj, L. Novotny, *Phys. Rev. Lett.* **2006**, *96*, 113002.

[54] A. L. Efros, M. Rosen, *Phys. Rev. Lett.* **1997**, *78*, 1110.

[55] D. W. de Quilettes, W. Zhang, V. M. Burlakov, D. J. Graham, T. Leijtens, A. Osherov, V. Bulović, H. J. Snaith, D. S. Ginger, S. D. Stranks, *Nat. Commun.* **2016**, *7*, 11683.

[56] a) W.-J. Yin, T. Shi, Y. Yan, *Appl. Phys. Lett.* **2014**, *104*, 063903; b) A. Buin, P. Pietsch, J. Xu, O. Voznyy, A. H. Ip, R. Comin, E. H. Sargent, *Nano Lett.* **2014**, *14*, 6281.

[57] M. L. Agiorgousis, Y.-Y. Sun, H. Zeng, S. Zhang, *J. Am. Chem. Soc.* **2014**, *136*, 14570.

[58] C. Qiu, J. K. Grey, *J Phys. Chem. Lett.* **2015**, *6*, 4560.

[59] C. Li, A. Guerrero, Y. Zhong, S. Huettner, *J. Phys: Condens. Matter* **2017**, *29*, 193001.

[60] a) Y. Shao, Y. Fang, T. Li, Q. Wang, Q. Dong, Y. Deng, Y. Yuan, H. Wei, M. Wang, A. Gruverman, J. Shield, J. Huang, *Energy Environ. Sci.* **2016**, *9*, 1752; b) J. S. Yun, J. Seidel, J. Kim, A. M. Soufiani, S. Huang, J. Lau, N. J. Jeon, S. I. Seok, M. A. Green, A. Ho-Baillie, *Adv. Energy Mater.* **2016**, *6*, 1600330.

[61] E. Mosconi, D. Meggiolaro, H. J. Snaith, S. D. Stranks, F. De Angelis, *Energy Environ. Sci.* **2016**, *9*, 3180.

[62] a) J. Song, J. Li, X. Li, L. Xu, Y. Dong, H. Zeng, *Adv. Mater.* **2015**, *27*, 7162; b) G. Li, F. W. R. Rivarola, N. J. L. K. Davis, S. Bai, T. C. Jellicoe, F. de la Peña, S. Hou, C. Ducati, F. Gao, R. H. Friend, N. C. Greenham, Z.-K. Tan, *Adv. Mater.* **2016**, *28*, 3528.

[63] V. K. Ravi, G. B. Markad, A. Nag, *ACS Energy Lett.* **2016**, *1*, 665.